Giant Enhancement of Rotation Sensing with $\mathcal{PT}$-Symmetric Circular Bragg Lasers

Ziyao Feng and Xiankai Sun*

Department of Electronic Engineering, The Chinese University of Hong Kong, Shatin, New Territories, Hong Kong

(Received 2 October 2019; revised manuscript received 22 March 2020; accepted 24 March 2020; published 29 May 2020)

$\mathcal{PT}$-symmetric systems can be used as ultrasensitive sensors by exploiting the non-Hermitian degeneracy at the exceptional point. However, operating and controlling these systems at the exceptional point are usually difficult. Here, we study the effect of rotation on threshold gain of circular Bragg lasers with radial $\mathcal{PT}$ symmetry. We find that, even deviating away from the exceptional point, these lasers can provide a two-orders-of-magnitude enhancement in the rotation sensitivity compared with the conventional circular Bragg lasers of similar geometry and threshold gain. Additionally, these lasers are more robust against perturbation in operating condition than sensors that must operate at the exceptional point.

DOI: 10.1103/PhysRevApplied.13.054078

I. INTRODUCTION

It is well known that most rotation sensors are based on the Sagnac effect, which refers to the different accumulated phases of light propagating along or against the rotation direction [1]. Fiber-optic gyroscopes feature high precision and reliability but they have relatively large sizes [2]. As basic components of photonic integrated circuits, photonic ring and disk resonators are widely used in rotation sensing to overcome the size limitation [3–6]. Passive and active photonic resonators can both be used for gyroscopes. However, detecting the signals induced by the Sagnac effect for on-chip devices is sometimes challenging [5,7,8]. It was found that in addition to the well-known Sagnac effect, the threshold gain of ring or disk lasers will also change with rotation, as reported in Ref. [9]. Circular Bragg lasers are an ideal candidate for rotation sensing due to their inherent advantages, such as cylindrically symmetric geometry and large emission aperture [9–13]. The rotation-induced change of threshold gain is actually more significant than the frequency shift, and this effect is more pronounced in the ring or disk lasers laterally confined by distributed Bragg reflection than by total internal reflection [9]. In addition to rotation sensing, other rotation-related phenomena and applications have also been explored, including optomechanically induced transparency [14,15] and quantum nonreciprocity [16,17].

The concept of "$\mathcal{PT}$ symmetry" was proposed by Bender *et al*. to investigate systems with a non-Hermitian Hamiltonian [18]. A $\mathcal{PT}$-symmetric system can have real eigenvalues in the $\mathcal{PT}$-symmetric phase and complex eigenvalues in the $\mathcal{PT}$-broken phase. The two phases are separated by the exceptional point. $\mathcal{PT}$-symmetric systems have also been theoretically analyzed and experimentally demonstrated in photonics and mechanics [19,20], leading to many interesting phenomena such as enhanced modal discrimination [12,21], phonon lasing [22–25] and cooling [26], reversed or nonreciprocal optomechanically induced transparency [27–29], quantum nonreciprocity [30], orbital angular-momentum lasing [31], unidirectional reflection [32,33], and enhanced sensing near the exceptional point [34,35]. However, the reported enhanced sensing is based on the non-Hermitian degeneracies at the exceptional point, which is usually difficult to implement experimentally.

Previously, we proposed a $\mathcal{PT}$-symmetric circular Bragg laser structure as shown in Fig. 1(a), where a disk is surrounded by a radial $\mathcal{PT}$-symmetric grating [12]. In the grating region, the real and imaginary parts of the refractive index are designed to follow the distributions of the Hankel functions (the eigenwaves in the cylindrical coordinates). Our previous analyses concluded that such structures can have higher modal discrimination than the conventional circular Bragg lasers whose gratings consist of modulation of only the real part of the refractive index [12]. In 2007, Scheuer *et al*. investigated the effect of rotation on the lasing properties of conventional circular Bragg lasers, and found that rotation affects not only the resonant frequencies but also the threshold gain of the resonant modes [9]. Here, we explore the effect of rotation on the threshold gain of circular Bragg lasers with radial $\mathcal{PT}$ symmetry and compare their sensing sensitivity with other types of rotation sensors. Compared with other proposals for weak-signal detection [36–38], our

*xksun@cuhk.edu.hk

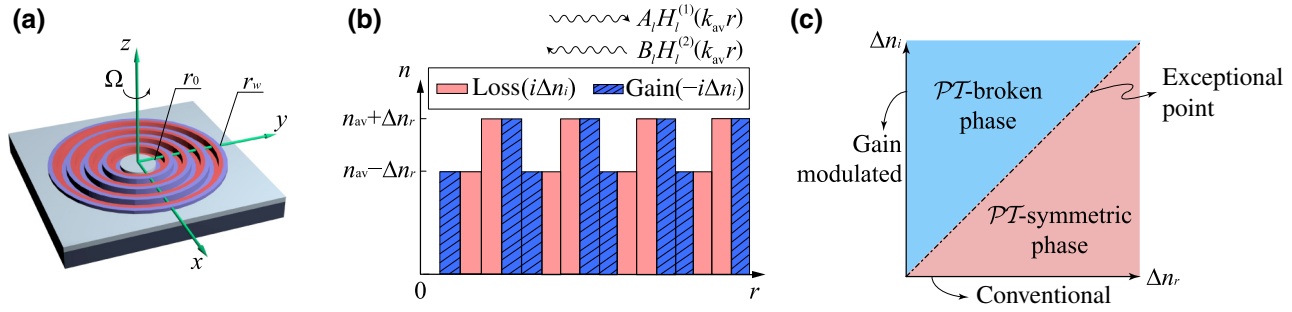

FIG. 1. (a) Schematic illustration of a $\mathcal{PT}$-symmetric circular Bragg laser. (b) Distribution of refractive index in the radial direction, showing that the real and imaginary refractive-index modulations satisfy the $\mathcal{PT}$ symmetry. (c) Classification of $\mathcal{PT}$-symmetric circular Bragg lasers according to the values of Δn_r and Δn_i.

proposed rotation sensors can have both high sensitivity and robust performance against environmental variations (e.g., temperature variations).

This Paper is structured as follows: Section II presents the theory with the calculated normalized threshold gain and sensitivity for circular Bragg lasers. Section III analyzes the rotation-induced variation of resonant frequency and threshold gain for circular Bragg lasers of three different types, namely, the "conventional," "exceptional point," and "gain modulated," which are classified based on the type of modulation of their complex refractive index. Section IV discusses possible ways to further enhance the rotation sensitivity and analyzes the effect of slight deviation from the designed operation. Section V concludes this Paper.

II. THEORETICAL FORMALISM

Without loss of generality, we focus on an azimuthal mode of a circular Bragg laser structure with perturbation in the radial direction [9,12,39]. Both the TE and TM modes exist, which can be analyzed separately with a similar method. For the TM mode, whose E_z is the major field component, the other field components can be derived from E_z. If the rotation speed Ω is much less than $c/R_{\max}$ ($R_{\max}$ is the maximal distance between the structure and the rotation center), the relativistic effect can be ignored. Following the derivation in Ref. [39], we can include the effect of rotation in the wave equation

$$\left\{r^2\frac{\partial^2}{\partial r^2}+r\frac{\partial}{\partial r}+\frac{\partial^2}{\partial\theta^2}+r^2k_0^2\left[\varepsilon(r,\theta)+2i\frac{\Omega}{\omega}\frac{\partial}{\partial\theta}\right]\right\}E_z=0, \tag{1}$$

where the center of rotation is the origin of the cylindrical coordinate system and the angular velocity vector is $\Omega\hat{z}$, ω ($=2\pi f$) is the angular frequency of light, $\varepsilon(r,\theta)$ is the distribution of the relative permittivity [39]. When the circular Bragg laser rotates with respect to its axis of symmetry (i.e., the z axis), the effect induced by rotation does not vary in the angular direction, and this is a common assumption in theoretical analyses [9,40,41]. In this case, E_z can be expressed as a linear combination of all the azimuthal modes $E_z=\sum_{l=-\infty}^{\infty}E_{zl}\exp(-il\theta)$ where $E_{zl}=A_l(r)H_l^{(1)}(kr)+B_l(r)H_l^{(2)}(kr)$ is the field distribution of the lth-order mode in the radial direction and $\exp(-il\theta)$ is the field distribution in the angular direction. $H_l^{(1)}$ ($H_l^{(2)}$) is the Hankel function of the first (second) kind, which represents the outgoing (incoming) wave with the azimuthal mode number l. $H_l^{(1)}$ and $H_l^{(2)}$ are complex conjugates of each other and form the basis for the propagating waves in the cylindrical coordinate system. Substituting E_z into Eq. (1) and taking the orthogonality of different azimuthal modes, we obtain

$$\left\{r^2\frac{\partial^2}{\partial r^2}+r\frac{\partial}{\partial r}-l^2+r^2k_0^2[\varepsilon(r)+2l\Omega/\omega]\right\}E_{zl}(r)=0. \tag{2}$$

As shown in Eq. (2), rotation of the circular Bragg laser induces a change in the relative permittivity by adding $2l\Omega/\omega$ to ε [9]. Therefore, we can use the same methods in Ref. [12] (i.e., transfer-matrix method or coupled-mode theory) to analyze the effect of rotation by only changing the permittivity. The effect of rotation depends on the azimuthal order and optical frequency. To obtain enhanced sensitivity, azimuthal modes of higher order are usually preferred [9,41]. In the following analysis, for comparison purposes, we choose the eighth azimuthal mode as previously investigated by Scheuer *et al.* [9,11]. The basic structure shown in Fig. 1(a) is composed of three sections, the inner disk ($r<r_0$), the Bragg grating with spatial frequency of k_{de} ($r_0<r<r_w$), and the outer region ($r>r_w$). Here, we describe the radial length L ($=r_w-r_0$) of the Bragg grating by referring to the number of periods of refractive-index modulation. The refractive index of the inner disk and outer region is n_{av}. The relative permittivity in the Bragg grating region is expressed as

$$\begin{aligned}\varepsilon=\varepsilon_{av}&-\Delta\varepsilon_r\text{sign}(\sin\{2\text{phase}[H_8^{(1)}(k_{de}r)]\})\\&-i\Delta\varepsilon_i\text{sign}(\cos\{2\text{phase}[H_8^{(1)}(k_{de}r)]\}),\end{aligned} \tag{3}$$

where $\varepsilon_{\rm av}$ is equal to $n_{\rm av}^2$, phase(x) denotes the phase of the complex variable x, and sign(x) is 1 for positive x and -1 for negative x. We obtain the coupled equations for the amplitudes of both the outgoing and incoming waves in the Bragg grating region [10]:

$$\begin{cases} \frac{dA_l}{dr} = \frac{-\Delta\varepsilon_r+\Delta\varepsilon_i}{4n_{\rm av}} k_0 B_l(r)\exp(-2i\delta r), \\ \frac{dB_l}{dr} = \frac{-\Delta\varepsilon_r-\Delta\varepsilon_i}{4n_{\rm av}} k_0 A_l(r)\exp(2i\delta r), \end{cases} \tag{4}$$

where $\delta = k_0 n_{\rm av} - k_{\rm de}$ is the detuning of the actual wave number from the spatial frequency of the relative permittivity in the radial direction. Assuming that at the outer boundary of the Bragg grating $B_l(r_w) = 0$, which means no incoming wave exists in the outer region, we obtain the amplitudes A_l and B_l at the inner boundary ($r = r_0$) and also the reflectivity for outgoing waves in the inner disk. In this way, the reflectivity for the eighth azimuthal mode with $\delta = 0$ is

$$R = \frac{(\kappa+g)[\exp(i\gamma L) - \exp(-i\gamma L)]}{[\exp(i\gamma L) + \exp(-i\gamma L)]i\gamma}, \tag{5}$$

where $\kappa = \Delta\varepsilon_r k_0/4n_{\rm av}$ and $g = \Delta\varepsilon_i k_0/4n_{\rm av}$ are the coupling strength due to modulation of the real and imaginary parts of the relative permittivity, respectively, and γ as the eigenvalue of Eq. (4) is defined as $\sqrt{\kappa^2 - g^2}$.

When the system works near the exceptional point ($\Delta\varepsilon_r \approx \Delta\varepsilon_i$), which is known to have enhanced sensitivity, we have $\gamma \ll \kappa$ and $\gamma \ll g$. In our analysis, we choose κ and g to be between 0 and 2.4×10^4 m^{-1}, L to be approximately 18 μm, and κL and gL to be less than 1, so that $|\gamma L| \ll \kappa L$, $|\gamma L| \ll gL$, and $|\gamma L| \ll 1$. By applying Euler's formula and the squeeze theorem, the reflectivity can be simplified as

$$R = (\kappa+g)\frac{\tan(i\gamma L)}{i\gamma} \approx (\kappa+g)L. \tag{6}$$

Based on the definition $\varepsilon = n^2 = (n_{\rm av} + \Delta n_r + i\Delta n_i)^2$, ε can be approximated as $n_{\rm av}^2 + 2n_{\rm av}\Delta n_r + 2in_{\rm av}\Delta n_i$ under the typical condition of $\Delta n_r \ll n_{\rm av}$ and $\Delta n_i \ll n_{\rm av}$. Therefore, with rotation the effective relative permittivity can be expressed as $n_{\rm av}^2 + 2l\Omega/\omega + 2n_{\rm av}\Delta n_r + 2in_{\rm av}\Delta n_i$, and the rotation-induced variation rate of reflectivity can be expressed as

$$\frac{dR}{d\Omega} = -\frac{(\Delta\varepsilon_r + \Delta\varepsilon_i)lk_0}{4\omega\varepsilon_{\rm av}^{3/2}}L = \frac{dR}{d\varepsilon_{\rm av}}\frac{2l}{\omega}. \tag{7}$$

Apparently, this variation rate is proportional to the rate at which the reflectivity changes with the relative permittivity. It should be noted that rotation will not affect the modulation depths $\Delta\varepsilon_r$ and $\Delta\varepsilon_i$ directly, as previously pointed out by Scheuer *et al.* [9].

Next, we study the system's sensing sensitivity. For the proposed structure, we choose the number of periods to be 50, r_0 to be 1.63 μm, and $n_{\rm av}$ to be 2.15. The laser oscillation condition is expressed as $R_0\exp(2i\delta r_0 + 2\alpha r_0)R = 1$, where R_0 the reflection coefficient at $r = 0$ must be 1, and α denotes the gain coefficient in the inner disk region ($r < r_0$). We may define the normalized threshold gain αr_0 as the gain required for light during its travel from the center to the edge of the inner disk to satisfy the laser oscillation condition. With $\delta = 0$, the normalized threshold gain can also be expressed as $\ln(R^{-1/2})$. Figure 2(a) shows the calculated normalized threshold gain for Δn_r from 0 to 0.2 and Δn_i from 0 to 0.02. Since rotation induces a change in the effective relative permittivity, the variation rate of the normalized threshold gain due to the change of effective relative permittivity $d\ln(R^{-1/2})/d\varepsilon_{\rm av}$ is defined as the sensitivity. Figure 2(b) shows the calculated sensitivity as a function of Δn_r and Δn_i. When the modulation of the refractive index occurs in only one quadrature, i.e., either the real or the imaginary part but not both, the reflectivity in Eq. (5) is expressed as $\tanh[\kappa(r_w - r_0)]$ when $\Delta n_i = 0$ and as $\tan[g(r_w - r_0)]$ when $\Delta n_r = 0$. The analytical expressions of sensitivity for the two special cases ($\Delta n_i = 0$ or $\Delta n_r = 0$) are

$$\left.\frac{d\ln(R^{-1/2})}{d\varepsilon_{\rm av}}\right|_{\Delta n_i = 0} = \frac{[\exp(\kappa L) + \exp(-\kappa L)]\Delta\varepsilon_r k_0 L}{8[1 - \exp(-2\kappa L)][1 + \exp(\kappa L)]^2\varepsilon_{\rm av}^{3/2}}, \tag{8}$$

$$\left.\frac{d\ln(R^{-1/2})}{d\varepsilon_{\rm av}}\right|_{\Delta n_r = 0} = \frac{\Delta\varepsilon_i k_0 L}{8\sin(2gL)\varepsilon_{\rm av}^{3/2}}. \tag{9}$$

It should be noted that κ (g) is linearly related to $\Delta\varepsilon_r$ ($\Delta\varepsilon_i$). According to Eq. (8), when $\Delta n_i = 0$, the sensitivity gradually decreases with increased modulation depth Δn_r, as shown in Fig. 2(c). According to Eq. (9), when $\Delta n_r = 0$, the sensitivity increases with increased modulation depth Δn_i, as shown in Fig. 2(d). Figure 2(a) shows that increasing the real or imaginary modulation depth yields decreased normalized threshold gain. For conventional circular Bragg lasers with only real modulation ($\Delta n_i = 0$), a larger modulation depth Δn_r leads to lower normalized threshold gain but meanwhile lower sensitivity. This challenge can be overcome by adding an imaginary modulation Δn_i to produce a $\mathcal{PT}$-symmetric circular Bragg laser. Maintaining the same normalized threshold gain, we can enhance the rotation sensitivity by increasing the imaginary modulation depth Δn_i while decreasing the real modulation depth Δn_r following the blue curve

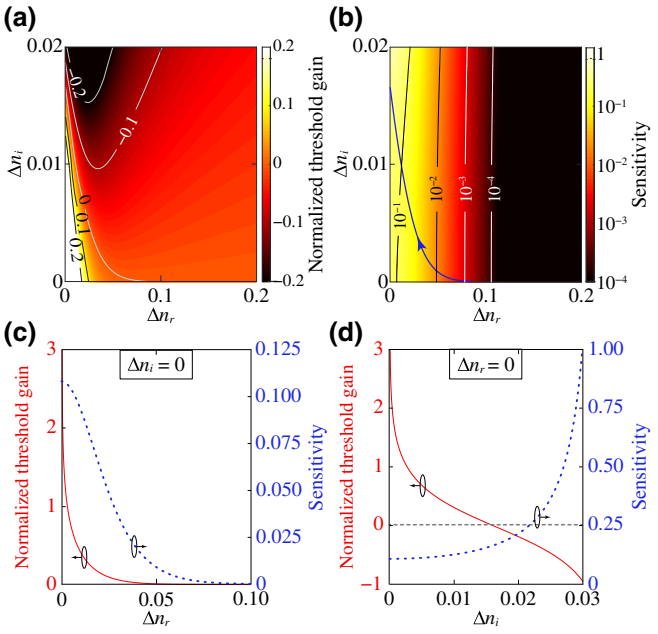

FIG. 2. (a), (b) Normalized threshold gain (a) and sensitivity (b) as a function of both the real and imaginary refractive-index modulation depths Δn_r and Δn_i. The blue curve with an arrow indicates a path to achieve enhanced rotation sensitivity while maintaining the same normalized threshold gain for structures of different Δn_r and Δn_i values. (c) Normalized threshold gain and sensitivity as a function of the real refractive-index modulation depth Δn_r under the condition of $\Delta n_i = 0$. (d) Normalized threshold gain and sensitivity as a function of the imaginary refractive-index modulation depth Δn_i under the condition of $\Delta n_r = 0$.

along the direction as indicated by the arrow in Fig. 2(b). It should be noted that the normalized threshold gain of $\mathcal{PT}$-symmetric circular Bragg lasers can be negative, while that of conventional circular Bragg lasers is always positive [42].

Figures 2(c) and 2(d) show that with the same normalized threshold gain, the sensitivity for the circular Bragg lasers with only imaginary modulation is massively enhanced from that with only real modulation. For example, when $\Delta n_i = 0$ and $\Delta n_r = 0.0816$, the normalized threshold gain is 4.5×10^{-4} and the sensitivity is 7.5×10^{-4}. However, when $\Delta n_r = 0$ and $\Delta n_i = 0.0167$, the normalized threshold gain is also 4.5×10^{-4} but the sensitivity is 0.1698, which is approximately 226 times larger than that for $\Delta n_i = 0$ and $\Delta n_r = 0.0816$. For a general $\mathcal{PT}$-symmetric circular Bragg laser with both real and imaginary modulation ($\Delta n_r \neq 0$, $\Delta n_i \neq 0$), the normalized threshold gain can be lower than that with only imaginary modulation ($\Delta n_r = 0$, $\Delta n_i \neq 0$), but the sensitivity is reduced. By tracing back to the dispersion relation $\gamma = \sqrt{\kappa^2 - g^2}$, one finds that a larger ratio between Δn_i and Δn_r leads the system to be situated more deeply in the $\mathcal{PT}$-broken region, thus having a higher sensitivity [12].

III. ROTATION-INDUCED FREQUENCY AND THRESHOLD GAIN VARIATION

The coupled-mode theory in the previous section is a perturbational approach, which is accurate under the condition of $\Delta n_r \ll n_{\mathrm{av}}$ and $\Delta n_i \ll n_{\mathrm{av}}$. For large modulation depths, the results derived from the coupled-mode theory deviate from the actual values. In this regard, the transfer-matrix method, which is based on the continuity of electric field and its derivative at the interfaces between adjacent layers, can be used instead to calculate the normalized threshold gain. During calculation, we choose a circular Bragg laser structure with the grating region consisting of 25 periods. We also choose r_0 as 1.63 μm and n_{av} as 2.15. The real and imaginary modulation depths are chosen to obtain similar threshold gain for the eighth azimuthal mode. Therefore, we choose $\Delta n_r = \Delta n_i = 0.020405$ corresponding to the $\mathcal{PT}$-symmetric laser working at the exceptional point to produce the normalized threshold gain of 4.35×10^{-4} and eigenfrequency of 1.9360×10^{14} Hz, $\Delta n_r = 0.1595$ and $\Delta n_i = 0$ corresponding to the conventional circular Bragg laser with only real modulation to produce the normalized threshold gain of 4.35×10^{-4} and eigenfrequency of 1.9437×10^{14} Hz, and $\Delta n_r = 0$ and $\Delta n_i = 0.03206$ corresponding to the gain-modulated circular Bragg laser with only imaginary modulation to produce the normalized threshold gain of 4.35×10^{-4} and eigenfrequency of 1.9357×10^{14} Hz. The clockwise (counterclockwise) rotation is defined as the positive (negative) rotation direction.

Figure 3(a) shows that the above three types ($\Delta n_i = 0$, $\Delta n_r = \Delta n_i$, and $\Delta n_r = 0$) of circular Bragg lasers have very similar response of resonant frequency to rotation speed, which is attributed to the Sagnac effect [9, 39,43]. By comparing Figs. 3(a) and 3(b), it can be

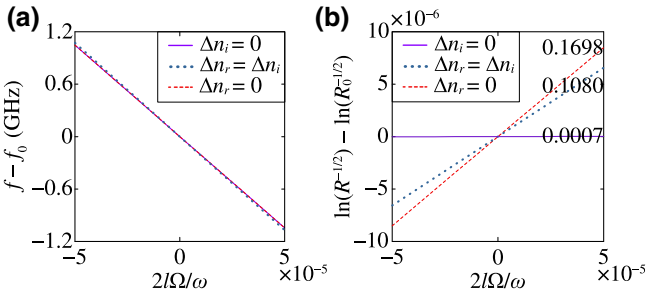

FIG. 3. (a) Dependence of modal frequency on the rotation speed $2l\Omega/\omega$ for the three types ($\Delta n_i = 0$, $\Delta n_r = \Delta n_i$, $\Delta n_r = 0$) of circular Bragg lasers. (b) Dependence of normalized modal threshold gain on the rotation speed $2l\Omega/\omega$ for the three types ($\Delta n_i = 0$, $\Delta n_r = \Delta n_i$, $\Delta n_r = 0$) of circular Bragg lasers. Numbers on the lines are the corresponding rotation sensitivities.

concluded that the relative change of normalized threshold gain $[\ln(R^{-1/2}) - \ln(R_0^{-1/2})]/\ln(R_0^{-1/2})$ is more pronounced than the relative change of resonant frequency $(f - f_0)/f_0$. For example, for the gain-modulated circular Bragg laser, the relative change of resonant frequency is 1.08×10^{-6} while the relative change of normalized threshold gain is 8.04×10^{-3} when $2l\Omega/\omega$ is 1×10^{-5}. Figure 3(b) also shows that the change of threshold gain induced by rotation is quite different for the three types of lasers. The sensitivity of the gain-modulated laser with pure imaginary modulation is massively enhanced from that of the conventional laser with pure real modulation. Actually, the sensitivity of the gain-modulated laser (0.1698) is approximately 243 times larger than that of the conventional circular Bragg laser (7.0×10^{-4}), and also approximately 1.6 times larger than that of the $\mathcal{PT}$-symmetric laser working at the exceptional point (0.1080). These results agree well with those from the coupled-mode theory.

Breaking the angular symmetry, the rotation leads to different effects on the threshold gain of the clockwise and counterclockwise modes. If the circular Bragg laser rotates clockwise, the threshold gain of the clockwise (counterclockwise) mode will increase (decrease) with the rotation speed. If the optical gain supplied to the inner disk is increased gradually, then different modes will lase in sequence, which can provide information of the threshold gain for each mode. Alternatively, under a high pump power beyond their thresholds, both modes will lase and the laser will operate in a steady state due to the gain saturation effect, where the intensities of the clockwise and counterclockwise modes will be different [13]. We can obtain the rotation speed by observing the interference pattern of the clockwise and counterclockwise modes.

IV. DISCUSSION

In the above analysis, to compare the three types of laser structures, we focus only on the cases where the normalized threshold gain is positive. Figures 2(b) and 2(d) as well as Eqs. (8) and (9) show that the sensitivity can be enhanced by increasing either the modulation depth Δn_i or the radial length of the circular Bragg grating L. Next, we focus on the gain-modulated laser structure with only imaginary modulation and use the transfer-matrix method to calculate the normalized threshold gain as a function of the rotation speed for different imaginary modulation depths, with the results shown in Fig. 4(a). It is clear that the rotation sensitivity increases with the modulation depth Δn_i. However, for large modulation depths, the threshold gain becomes negative [e.g., $\ln(R^{-1/2}) = -1$ for $\Delta n_i = 0.06$], which means that the laser already operates above the threshold due to the excessive gain from the circular Bragg grating. One can add additional loss to the inner disk region to bring the laser back to the threshold condition if necessary.

So far, our analysis has focused only on the ideal structures. In reality, the imaginary modulation is usually realized by patterned metal and optical pumping on a semiconductor gain material, so it is difficult to accurately control the imaginary part of the average refractive index n_{av} in the grating region. Here, we define n_{dev} as the deviation from the designed imaginary part of the average refractive index. A positive (negative) n_{dev} denotes more (less) loss than gain in the grating region. We choose the case where the imaginary modulation depth Δn_i is 0.03206. Figure 4(b) shows that as n_{dev} decreases, the sensitivity is enhanced. Compared with the cases with a positive n_{dev}, those with a negative n_{dev} have higher sensitivity due to net

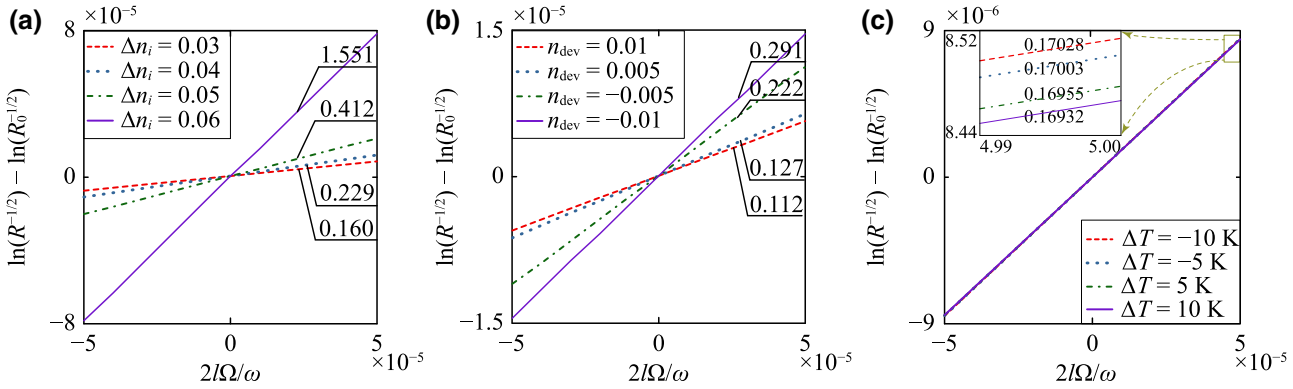

FIG. 4. (a) Dependence of normalized modal threshold gain of several gain-modulated circular Bragg laser structures ($\Delta n_r = 0$, $\Delta n_i = 0.03$, 0.04, 0.05, 0.06) on the rotation speed $2l\Omega/\omega$. (b) Dependence of normalized modal threshold gain of the gain-modulated circular Bragg laser structure ($\Delta n_r = 0$, $\Delta n_i = 0.03206$) on the rotation speed $2l\Omega/\omega$, where a slight deviation n_{dev} ($= 0.01$, 0.005, -0.005, -0.01) is added to the imaginary part of the average refractive index. (c) Dependence of normalized modal threshold gain of the gain-modulated circular Bragg laser structure ($\Delta n_r = 0$, $\Delta n_i = 0.03206$) on the rotation speed $2l\Omega/\omega$, where there is a slight temperature variation ΔT ($= -10$, -5, 5, 10 K). The inset is an enlarged plot for $2l\Omega/\omega \sim 5 \times 10^{-5}$. Numbers on the lines are the corresponding rotation sensitivities.

amplification of the optical fields in the grating region. On the other hand, it should be noted that our proposed structures are insensitive to temperature variations. Assuming that the system works at a temperature near 300 K and the thermo-optic coefficient is 2.02×10^{-4} K^{-1} [44], we calculate the normalized threshold gain as a function of the rotation speed for a slight temperature variation ΔT, with the results shown in Fig. 4(c). It is clear that the rotation sensitivity remains almost unchanged, which is an advantage of this type of rotation sensor compared with the traditional ones based on the Sagnac effect.

V. CONCLUSION

In conclusion, we propose and analyze a type of rotation sensor based on circular Bragg lasers by $\mathcal{PT}$-symmetry breaking. Different from other sensors, which perform best at the exceptional point, these rotation sensors can operate in the $\mathcal{PT}$-broken region with massively enhanced sensitivity. We first employ the coupled-mode theory to derive the rotation sensitivity for laser structures with real and/or imaginary refractive-index modulation. We find that with the same threshold gain, the sensitivity of the laser structures with pure imaginary modulation is massively enhanced from that of conventional laser structures with pure real modulation. We then adopt the transfer-matrix method to simulate the effect of rotation on the threshold gain of the lasers. We find that the gain-modulated laser structures feature massively enhanced sensitivity, which is approximately 243 times larger than that of conventional laser structures with the same normalized threshold gain of 4.35×10^{-4}. Additionally, a larger modulation depth Δn_i results in enhanced sensitivity, and a slight deviation in device fabrication and operation from the ideal condition will not affect the sensitivity significantly.

ACKNOWLEDGMENTS

This work is supported by the Early Career Scheme (Project No. 24208915) and the General Research Fund (Project No. 14208717, 14206318) sponsored by the Research Grants Council of Hong Kong, and by the NSFC/RGC Joint Research Scheme (Project No. N_CUHK415/15) sponsored by the Research Grants Council of Hong Kong and the National Natural Science Foundation of China.

APPENDIX: DETAILS OF TRANSFER-MATRIX METHOD

For analyzing circular Bragg lasers, the transfer-matrix method has been widely used to calculate the normalized threshold gain for a specific mode. We adopt the transfer matrices to relate the amplitudes of the outgoing and incoming waves in the inner disk region to the amplitudes of the outgoing and incoming waves in the outer region. It is convenient to consider the E_z-field component satisfying Eq. (1). When the center of rotation coincides with the origin of the cylindrical coordinate system and the angular velocity vector is $\Omega\hat{z}$, E_z of the lth-order mode also satisfies Eq. (2).

In a specific qth layer, the relative permittivity (ε_q) is a constant, so the solution of Eq. (2) can be expressed as a linear combination of the Hankel functions of the first and second kinds

$$E_{zl}^{q}(r) = A_l^q H_q^{(1)}(k_q r) + B_l^q H_q^{(2)}(k_q r), \tag{A1}$$

where k_q is the wavevector in the qth layer. The wavevector k_q is defined as $k_0\sqrt{\varepsilon_q + 2l\Omega/\omega}$. $H_q^{(1)}$ and $H_q^{(2)}$ represent the outgoing and incoming waves with amplitudes A_l^q and B_l^q, respectively. To build the connection between the amplitudes of outgoing and incoming waves in adjacent layers, the continuity of the electric field and its derivative at the interface is invoked. The derivative of the electric field can be written as

$$E_{zl}^{q\prime}(r) = A_l^q k_q H_q^{(1)\prime}(k_q r) + B_l^q k_q H_q^{(2)\prime}(k_q r). \tag{A2}$$

With r_q defined as the outer radius of the qth layer, E_{zl}^{q} defined in Eq. (A1), and $E_{zl}^{q\prime}$ defined in Eq. (A2), we obtain

$$\begin{aligned}\begin{bmatrix} A_l^{q+1} \\ B_l^{q+1} \end{bmatrix} &= \begin{bmatrix} H_{q+1}^{(1)}(k_{q+1}r_q) & H_{q+1}^{(2)}(k_{q+1}r_q) \\ k_{q+1}H_{q+1}^{(1)\prime}(k_{q+1}r_q) & k_{q+1}H_{q+1}^{(2)\prime}(k_{q+1}r_q) \end{bmatrix}^{-1} \\ &\quad \begin{bmatrix} H_q^{(1)}(k_q r_q) & H_q^{(2)}(k_q r_q) \\ k_q H_q^{(1)\prime}(k_q r_q) & k_q H_q^{(2)\prime}(k_q r_q) \end{bmatrix} \begin{bmatrix} A_l^q \\ B_l^q \end{bmatrix} \\ &= T_l^q \begin{bmatrix} A_l^q \\ B_l^q \end{bmatrix}, \end{aligned} \tag{A3}$$

where T_l^q is the transfer matrix between the qth layer and the $(q+1)$th layer. By multiplying the transfer matrices one by one, we establish a relation between the outgoing and incoming waves in the inner disk region (A_l^{in} and B_l^{in}) and those in the outer region (A_l^{out} and B_l^{out}):

$$\begin{aligned}\begin{bmatrix} A_l^{\text{out}} \\ B_l^{\text{out}} \end{bmatrix} &= T_l^N T_l^{N-1} \cdots T_l^1 T_l^0 \begin{bmatrix} A_l^{\text{in}} \\ B_l^{\text{in}} \end{bmatrix} \\ &= \begin{bmatrix} U_{11} & U_{12} \\ U_{21} & U_{22} \end{bmatrix} \begin{bmatrix} A_l^{\text{in}} \\ B_l^{\text{in}} \end{bmatrix}. \end{aligned} \tag{A4}$$

For the circular Bragg laser, the amplitude of the incoming wave (B_l^{out}) in the outer region is set to be 0. Equation (A4) can be simplified to $U_{21}A_l^{\text{in}} + U_{22}B_l^{\text{in}} = 0$, and the reflectivity of the outgoing wave of the lth-order mode ($B_l^{\text{in}}/A_l^{\text{in}}$) can be expressed as $-U_{21}/U_{22}$.

[1] E. J. Post, Sagnac effect, Rev. Mod. Phys. **39**, 475 (1967).
[2] H. C. Lefevre, *The Fiber-Optic Gyroscope* (Artech House, Norwood, 2014).
[3] K. J. Vahala, Optical microcavities, Nature **424**, 839 (2003).
[4] J. Li, M.-G. Suh, and K. Vahala, Microresonator Brillouin gyroscope, Optica **4**, 346 (2017).
[5] P. P. Khial, A. D. White, and A. Hajimiri, Nanophotonic optical gyroscope with reciprocal sensitivity enhancement, Nat. Photonics **12**, 671 (2018).
[6] J. Scheuer and A. Yariv, Sagnac Effect in Coupled-Resonator Slow-Light Waveguide Structures, Phys. Rev. Lett. **96**, 053901 (2006).
[7] B.-B. Li, J. Bílek, U. B. Hoff, L. S. Madsen, S. Forstner, V. Prakash, C. Schäfermeier, T. Gehring, W. P. Bowen, and U. L. Andersen, Quantum enhanced optomechanical magnetometry, Optica **5**, 850 (2018).
[8] J. Ahn, Z. Xu, J. Bang, P. Ju, X. Gao, and T. Li, Ultrasensitive torque detection with an optically levitated nanorotor, Nat. Nanotechnol. **15**, 89 (2020).
[9] J. Scheuer, Direct rotation-induced intensity modulation in circular Bragg micro-lasers, Opt. Express **15**, 15053 (2007).
[10] T. Erdogan and D. G. Hall, Circularly symmetric distributed feedback semiconductor laser: An analysis, J. Appl. Phys. **68**, 1435 (1990).
[11] J. Scheuer and A. Yariv, Coupled-waves approach to the design and analysis of Bragg and photonic crystal annular resonators, IEEE J. Quantum Electron. **39**, 1555 (2003).
[12] Z. Feng, J. Ma, Z. Yu, and X. Sun, Circular Bragg lasers with radial PT symmetry: Design and analysis with a coupled-mode approach, Photonics Res. **6**, A38 (2018).
[13] X. Sun and A. Yariv, Surface-emitting circular DFB, disk-, and ring-Bragg resonator lasers with chirped gratings. III: Gain saturation effects and above-threshold analysis, Opt. Express **17**, 10119 (2009).
[14] H. Lü, Y. Jiang, Y.-Z. Wang, and H. Jing, Optomechanically induced transparency in a spinning resonator, Photonics Res. **5**, 367 (2017).
[15] Z. Shen, Y.-L. Zhang, Y. Chen, C.-L. Zou, Y.-F. Xiao, X.-B. Zou, F.-W. Sun, G.-C. Guo, and C.-H. Dong, Experimental realization of optomechanically induced non-reciprocity, Nat. Photonics **10**, 657 (2016).
[16] S. Maayani, R. Dahan, Y. Kligerman, E. Moses, A. U. Hassan, H. Jing, F. Nori, D. N. Christodoulides, and T. Carmon, Flying couplers above spinning resonators generate irreversible refraction, Nature **558**, 569 (2018).
[17] R. Huang, A. Miranowicz, J.-Q. Liao, F. Nori, and H. Jing, Nonreciprocal Photon Blockade, Phys. Rev. Lett. **121**, 153601 (2018).
[18] C. M. Bender and S. Boettcher, Real Spectra in Non-Hermitian Hamiltonians Having PT Symmetry, Phys. Rev. Lett. **80**, 5243 (1998).
[19] A. Guo, G. J. Salamo, D. Duchesne, R. Morandotti, M. Volatier-Ravat, V. Aimez, G. A. Siviloglou, and D. N. Christodoulides, Observation of PT-Symmetry Breaking in Complex Optical Potentials, Phys. Rev. Lett. **103**, 093902 (2009).
[20] R. Fleury, D. Sounas, and A. Alù, An invisible acoustic sensor based on parity–time symmetry, Nat. Commun. **6**, 5905 (2015).
[21] L. Feng, Z. J. Wong, R.-M. Ma, Y. Wang, and X. Zhang, Single-mode laser by parity–time symmetry breaking, Science **346**, 972 (2014).
[22] H. Jing, S. K. Özdemir, X.-Y. Lü, J. Zhang, L. Yang, and F. Nori, PT-Symmetric Phonon Laser, Phys. Rev. Lett. **113**, 053604 (2014).
[23] H. Lü, S. K. Özdemir, L. M. Kuang, F. Nori, and H. Jing, Exceptional Points in Random-Defect Phonon Lasers, Phys. Rev. Appl. **8**, 044020 (2017).
[24] J. Zhang, B. Peng, Ş. K. Özdemir, K. Pichler, D. O. Krimer, G. Zhao, F. Nori, Y.-x. Liu, S. Rotter, and L. Yang, A phonon laser operating at an exceptional point, Nat. Photonics **12**, 479 (2018).
[25] Y. Jiang, S. Maayani, T. Carmon, F. Nori, and H. Jing, Nonreciprocal Phonon Laser, Phys. Rev. Appl. **10**, 064037 (2018).
[26] H. Jing, Ş. K. Özdemir, H. Lü, and F. Nori, High-order exceptional points in optomechanics, Sci. Rep. **7**, 3386 (2017).
[27] H. Jing, Ş. K. Özdemir, Z. Geng, J. Zhang, X.-Y. Lü, B. Peng, L. Yang, and F. Nori, Optomechanically-induced transparency in parity–time-symmetric microresonators, Sci. Rep. **5**, 9663 (2015).
[28] W. Li, Y. Jiang, C. Li, and H. Song, Parity–time-symmetry enhanced optomechanically-induced-transparency, Sci. Rep. **6**, 31095 (2016).
[29] H. Lü, C. Wang, L. Yang, and H. Jing, Optomechanically Induced Transparency at Exceptional Points, Phys. Rev. Appl. **10**, 014006 (2018).
[30] Ş. K. Özdemir, S. Rotter, F. Nori, and L. Yang, Parity–time symmetry and exceptional points in photonics, Nat. Mater. **18**, 783 (2019).
[31] P. Miao, Z. Zhang, J. Sun, W. Walasik, S. Longhi, N. M. Litchinitser, and L. Feng, Orbital angular momentum microlaser, Science **353**, 464 (2016).
[32] K. G. Makris, R. El-Ganainy, D. N. Christodoulides, and Z. H. Musslimani, Beam Dynamics in PT Symmetric Optical Lattices, Phys. Rev. Lett. **100**, 103904 (2008).
[33] Z. Feng, J. Ma, and X. Sun, Parity–time-symmetric mechanical systems by the cavity optomechanical effect, Opt. Lett. **43**, 4088 (2018).
[34] H. Hodaei, A. U. Hassan, S. Wittek, H. Garcia-Gracia, R. El-Ganainy, D. N. Christodoulides, and M. Khajavikhan, Enhanced sensitivity at higher-order exceptional points, Nature **548**, 187 (2017).
[35] W. Chen, Ş Kaya Özdemir, G. Zhao, J. Wiersig, and L. Yang, Exceptional points enhance sensing in an optical microcavity, Nature **548**, 192 (2017).
[36] Z.-P. Liu, J. Zhang, ŞK Özdemir, B. Peng, H. Jing, X.-Y. Lü, C.-W. Li, L. Yang, F. Nori, and Y.-x. Liu, Metrology with PT-Symmetric Cavities: Enhanced Sensitivity Near the PT-Phase Transition, Phys. Rev. Lett. **117**, 110802 (2016).
[37] H. Jing, H. Lü, S. K. Özdemir, T. Carmon, and F. Nori, Nanoparticle sensing with a spinning resonator, Optica **5**, 1424 (2018).
[38] Q. Zhong, J. Ren, M. Khajavikhan, D. N. Christodoulides, Ş. K. Özdemir, and R. El-Ganainy, Sensing with Exceptional Surfaces in Order to Combine Sensitivity with

Robustness, Phys. Rev. Lett. **122**, 153902 (2019).
[39] S. Sunada and T. Harayama, Sagnac effect in resonant microcavities, Phys. Rev. A **74**, 021801 (2006).
[40] R. Sarma, L. Ge, J. Wiersig, and H. Cao, Rotating Optical Microcavities with Broken Chiral Symmetry, Phys. Rev. Lett. **114**, 053903 (2015).
[41] L. Ge, R. Sarma, and H. Cao, Rotation-induced evolution of far-field emission patterns of deformed microdisk cavities, Optica **2**, 323 (2015).
[42] J. Gu, X. Xi, J. Ma, Z. Yu, and X. Sun, Parity–time-symmetric circular Bragg lasers: A proposal and analysis, Sci. Rep. **6**, 37688 (2016).
[43] R. Sarma, H. Noh, and H. Cao, Wavelength-scale microdisks as optical gyroscopes: A finite-difference time-domain simulation study, J. Opt. Soc. Am. B **29**, 1648 (2012).
[44] E. Gini and H. Melchior, Thermal dependence of the refractive index of InP measured with integrated optical demultiplexer, J. Appl. Phys. **79**, 4335 (1996).